Journal of Magnetism and Magnetic Materials 327 (2013) 11–19

Contents lists available at SciVerse ScienceDirect

Journal of Magnetism and Magnetic Materials

journal homepage: www.elsevier.com/locate/jmmm

Structural and magnetic properties of $Fe_{2-x}CoSm_xO_4$—nanoparticles and $Fe_{2-x}CoSm_xO_4$—PDMS magnetoelastomers as a function of Sm content

Mariano M. Ruiz [a], José L. Mietta [a], P. Soledad Antonel [a], Oscar E. Pérez [b], R. Martín Negri [a], Guillermo Jorge [c,d,*]

[a] Instituto de Química Física de Materiales, Ambiente y Energía (INQUIMAE), Departamento de Química Inorgánica, Analítica y Química Física, Facultad de Ciencias Exactas y Naturales, Universidad de Buenos Aires, Av. Cantilo s/n (1428), Buenos Aires, Argentina
[b] Departamento de Industrias, Facultad de Ciencias Exactas y Naturales, Universidad de Buenos Aires, Av. Cantilo s/n (1428), Buenos Aires, Argentina
[c] Instituto de Física de Buenos Aires, Facultad de Ciencias Exactas y Naturales, Universidad de Buenos Aires, Av. Cantilo s/n (1428), Buenos Aires, Argentina
[d] Instituto de Ciencias, Universidad Nacional de General Sarmiento, J.M. Gutiérrez 1150 (1613), Los Polvorines, Buenos Aires, Argentina

ARTICLE INFO

Article history:
Received 1 June 2012
Received in revised form
24 August 2012
Available online 16 September 2012

Keywords:
Magnetoelastomers
Magnetorheoelastomers
Magnetic nanoparticles
Magnetic composites

ABSTRACT

We have synthesized magnetic $Fe_{2-x}CoSm_xO_4$ nanoparticles (NPs) by means of the coprecipitation method, varying Sm content from $x=0$ to $x=0.5$. Energy-dispersive X-ray spectroscopy showed agreement between the metal proportion of the obtained nanoparticles and the stoichiometric mixture of cations used for the synthesis. Part of the particles were heated at 800 °C, and both were characterized by X-ray diffraction, scanning electron microscope imaging and magnetization measurements. Physical and magnetic properties were analyzed as a function of Sm content, before and after the heating treatment. A phase segregation is found for the calcined nanoparticles with large Sm content. The magnetic remanence, saturation and coercive field were investigated as a function of Sm content for both heated and unheated (as-prepared) particles. Polydimethylsiloxane-NPs magnetoelastomers were prepared and cured under an external uniform magnetic field, obtaining structured anisotropic composites, in which inorganic needles (columnar micrometric structures) oriented in the direction of the magnetic field are formed. Young modulus and remanent magnetic moment were measured and magnetization time relaxation experiments were performed in the directions parallel and perpendicular to the needles in order to determine the magnetic and elastic anisotropy of the composites. The elastic modulus measured parallel to the needles resulted almost twice in magnitude with respect to the perpendicular modulus. The measured magnetic anisotropy of the composites is probably due to the enhanced interparticle interaction within a needle and the freezing of an preferred easy axis distribution among the particles at the curing process.

1. Introduction

Magnetic nanoparticles have a wide range of applications in modern science. In medicine, for example, they have a potential use for cancer treatment therapy[1,2] and magnetic resonance imaging and drug delivery[3]. In addition, they are used in elaboration of ferrofluids and magnetorheoelastomers, in which the nanostructures are dispersed in an high viscosity fluid such as silicon oil[4], resins or polymers[5], which have important applications in stiffness suppressors[6], acceleration sensors[7], and valves for microfluidic[8,9]. The resin or polymer can be cured under a uniform magnetic field, producing an ordered uniaxial magnetic structure of the magnetic material. The resulting composites hold very interesting structural and magnetic anisotropic properties[10].

In the design and testing of potentially interesting magnetorheoleastomers it is necessary to know the magnetic properties of the building magnetic nanostructures, as well as how they could be varied, in order to obtain the desired magnetic or elastic behavior. Particularly, in cobalt ferrites part of the Fe content can be substituted by samarium (Sm), changing their magnetic behavior. It could be a mechanism to tune magnetic properties in magnetoelastomers with potential technological applications. Nevertheless, up to our knowledge, there is no comprehensive study on the magnetic properties of Sm-substituted cobalt ferrites[11].

Many synthetic methods are reported in the literature as organic acid precursor [11], hydrothermal [12], and coprecipitation method [13–15]. In particular, the coprecipitation method is

* Correspondence to: Departamento de Física, UBA. Ciudad Universitaria, Pabellón I (C1428EGA), Buenos Aires, Argentina. Tel.: +54 11 4576 3300; fax: +54 11 4576 3357.
E-mail address: gjorge@df.uba.ar (G. Jorge).

0304-8853/$ - see front matter © 2012 Elsevier B.V. All rights reserved.
http://dx.doi.org/10.1016/j.jmmm.2012.09.020

a very simple and clean way to synthesize nanoparticles, it does not involve organic compounds and the remaining salts can be easily removed by washing with deionized water.

In this work, we present an encompassing study of the structural and magnetic properties of $Fe_{2-x}CoSm_xO_4$ with Sm content (x) between $x=0$ and $x=0.5$. The particles were prepared by the coprecipitation method, and were studied by means of X-ray Diffraction (XRD), scanning electron microscope (SEM) and transmition electron microscope (TEM) imaging, and magnetization measurements. With the obtained particles we develop anisotropic magnetoelastomers, dispersing the particles in uncured polydimethylsiloxane (PDMS) and curing under a uniform magnetic field. The elastic and magnetic anisotropic properties of the composites were studied in order to determine the magnetic and elastic anisotropies due to the spatial organization of particles within the composite.

2. Materials and methods

2.1. Synthesis of $Fe_{2-x}CoSm_xO_4$ nanoparticles

The nanoparticles (NPs) were synthesized by the coprecipitation method. Adapting from Antonel et al. [14] and *Mietta* et al. [15], stock solutions of $FeCl_3 \cdot 6H_20$ (1 M) and $CoCl_2 \cdot 6H_20$ (0.5 M) were prepared, both in HCl 0.4 M. For every batch of synthesized particles a mixture solution was prepared using stoichiometric volumes of acidic Fe(III) and Co(II) solutions, and samarium (III) oxide (Sm_2O_3) was dissolved in a stoichiometric ratio of concentrated HCl and filled with distilled water to complete a concentration of HCl of 0.4 M and final volume of 10 mL. The resulting acidic solution with the metals was slowly added (1 drop per 4 s) to 200 mL of 1.5 M NaOH solution at high speed stirring. The synthesis temperature (80 °C) was controlled by a water-jacketed reaction vessel with circulating thermostatic bath. Once finished the addition of the acidic solution, the system was left at 80 °C with high speed stirring to in order to homogenize the particle size. The obtained particles were separated from the reaction medium by centrifugation (12,000 G for 10 min) and then washed with Milli-Q water. Centrifugation-washing cycles were repeated until the pH of the supernatant was nearly 7 (about 6 cycles). Finally the particles were dried in a vacuum oven at 40 °C for 24 h.

Part of the obtained particles were calcined for 2 h in a furnace at 800 °C (heat rate of 4 °C/min) in order to increase the crystallinity degree and study its influence in phase, size, morphology and magnetic properties.

2.2. Preparation of PDMS-$Fe_{2-x}CoSm_xO_4$ composites

Details of the synthesis of structured PDMS-nanoparticles were given in previous works[14,15]. The base polymer and the cross linker agent were mixed in 10:1 ratio, and then the inorganic nanoparticles were added (10% w/w). The obtained mixture, still fluid, was poured in a cylindrical mold (a specially designed device, 1 cm diameter × 3 cm long) and placed between the magnetic poles of a Varian Low Impedance Electromagnet (model V3703)[15]. This equipment provides an homogeneous magnetic fields (the magnetic field used in all the preparations was 3.5 kOe) as the mould was rotated at 30 rpm and heated at (75 ± 5) °C for 4 h. Four different PDMS-NPs composites were prepared, using NPs of different composition ($x=0.1$; 0.2; 0.3 not calcined NPs and $x=0.1$ calcined NPs) in order to study the influence of the NPs composition and degree of crystallinity on the magnetoelastomer's properties.

2.3. Instrumentation

XRD analysis were performed with a Philips X-Pert diffractometer using Cu Kα radiation ($\lambda=1.54056$ Å). The average crystalline domain sizes were calculated with the Debye-Scherrer equation. TEM images were taken with Philips EM 301 equipment, SEM images and EDS analysis were obtained with a field Emission Scanning Electron Microscope (Zeiss Supra 40 Genimi). The average particle size was determined by counting 300 (or more) particles and the size distribution was fitted to log-normal curves.

Magnetic hysteresis curves and time relaxation of the remanent magnetization were measured with a Vibrating Sample Magnetometer (LakeShore 7400) at room temperature.

For elastic measurements and Young's modulus determination Stable Microsystems TA-XT2i Texture Analyzer equipment was used. This equipment compresses the sample at constant speed (0.1 mm/s) up to a given percentage of the initial thickness (usually 20 or 30%). A specially designed device was used for cutting the PDMS-$Fe_{2-x}CoSm_xO_4$ composites which allows obtaining axial and transverse slides with approximately the same area (0.83 and 0.79 cm^2 respectively) and equal thickness (3 mm).

3. Results and Discussions

3.1. SEM and TEM imaging

SEM images of the obtained particles before and after the heat treatment are shown on Fig. 1 (additional SEM images are shown in supplementary material, available online). The morphology of the non-calcined particles resulted to be of irregular spheres for all Sm(III) proportions and the particles tend to form micrometric aggregates due to magnetic interactions. For the calcined particles the SEM images show sharp borders forming very well defined nanocrystalline structures.

The average particle size was determined using SEM and TEM images, and all the particles follow a log-normal size distribution. The average sizes obtained by TEM are in excellent agreement with the values obtained from SEM imaging (TEM images are not shown). In Fig. 2 we show the average sizes for both series of particles. For the non-calcined particles, compared to Fe_2CoO_4 particles, the average particle size increases with small amounts of Sm(III) and reaches a maximum size of 36 nm when $x=0.1$. For higher Sm(III) contents ($x=0.15$–0.4) the average particle size decreases (except for $x=0.5$). For the particles exposed to heat treatment there is a similar tendency: the largest size resulted to be for $Fe_{1.9}CoSm_{0.1}O_4$ particles (32.5 nm), then the particle size became smaller when increasing Sm(III) content ($x=0.15$–0.5).

The average composition of all the synthesized particles was determined by energy-dispersive X-ray spectroscopy (EDS). The average proportion of Fe(III) and Sm(III) respect to Co(II) in all cases agrees with the stoichiometric composition. Only for large amounts of Sm(III) ($x=0.5$), a deviation for Fe(III) content respect Co(II) in particles before and after calcination is observed (see supplementary material).

3.2. Structure analysis

On Fig. 3a we present the XRD patterns for the obtained nanoparticles without calcining. For all compositions ($x=0$–0.5) the diffraction peaks can be assigned to the inverse spinel structure of Fe_2CoO_4 (JCPDF 22-1086). No other phases are observed even for large amounts of Sm(III). The XRD patterns of the calcined particles are shown on Fig. 3b. For small amounts of

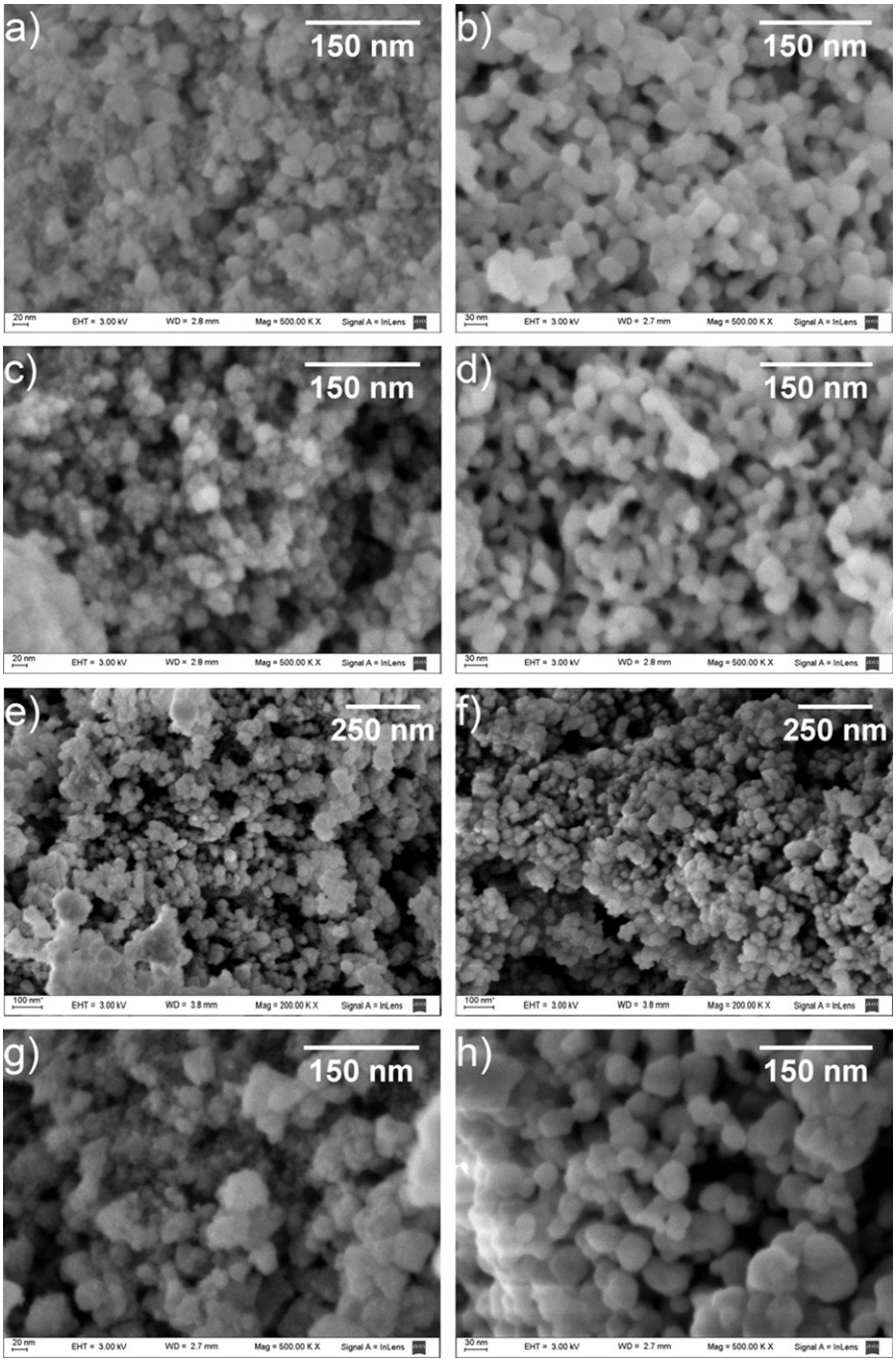

Fig. 1. SEM micrographs of $Fe_{2-x}CoSm_xO_4$ particles for different content of Sm before calcination: (a) $x=0$; (c) $x=0.05$; (e) $x=0.1$; (g) $x=0.15$; and after calcination: (b) $x=0$; (d) $x=0.05$; (f) $x=0.1$; (h) $x=0.15$.

Sm(III) ($x=0$–0.2) also an inverse spinel structure can be assigned, but for high content of Sm(III) ($x=0.3$–0.5) other stable phase seems to appear. According to other works[16,17] it can be attributed to a $FeSmO_3$ perovskite phase, with peaks at 31.5; 46; 47 and 49 degrees (ICDD JCPDF 74-1474).

Comparing the XRD patterns of the particles before and after calcination, it can be observed that the diffraction peaks become narrower after the heat treatment. Debye-Scherrer equation was used for calculating the average crystallite size using the most intense diffraction peak (311). On Table 1 the values of the lattice parameter and the average crystallite size for all the designed compositions, before and after the heat treatment, are presented. In all cases the average crystallite size determined by Debye-Scherrer increased after calcination at 800 °C. On the other hand, the lattice parameter decreased marginally for all the designed compositions after the heat treatment. After calcination at 800 °C, and for low Sm(III) content the lattice parameter remains approximately constant, but for higher Sm(III) content ($x=0.3$–0.5) there is a slightly decrease in the lattice parameter. Comparing the lattice parameter as a function of Sm content (x), it can be observed a similar tendency as the reported by *Peng* et al.[18].

In Fig. 4(a) we present the variation of the average crystallite size, determined by Debye-Scherrer equation as a function of Sm content for both series of particles. Both behave in a similar manner: At first the crystallite size decreases with a small amount of dopant (compared to Fe_2CoO_4 particles), then it increases until a maximum is reached when $x=0.15$; and for higher Sm(III) contents ($x=0.2$–0.5) the crystallite size decreases. Such change

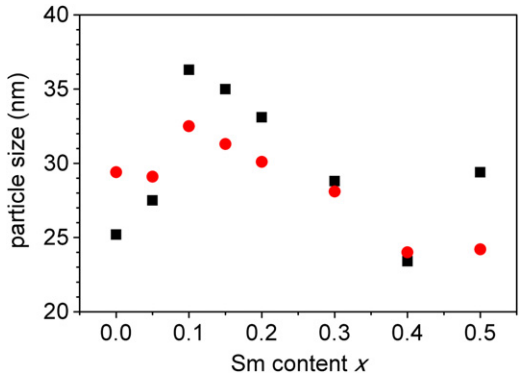

Fig. 2. Average particle size of $Fe_{2-x}CoSm_xO_4$ particles for different Sm content x, before (■) and after (●) calcination at 800 °C.

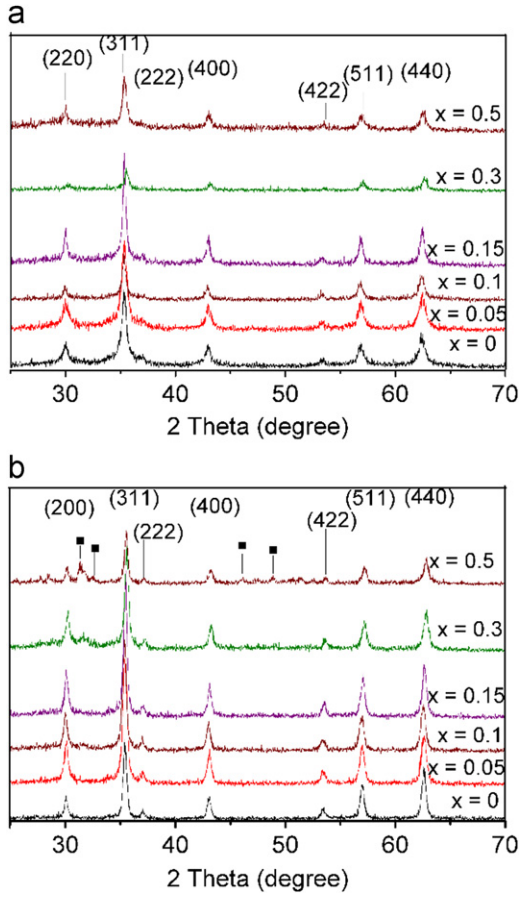

Fig. 3. (a) XRD patterns for the obtained $Fe_{2-x}CoSm_xO_4$ nanoparticles. All the peaks were assigned to inverse spinel structure. (b) XRD patterns of the nanoparticles after calcinations at 800 °C. For Sm content x higher than 0.3 a perovskite phase (■) of $FeSmO_3$ appears.

of behavior for $x > 0.2$ can be an indication of the segregation of a new structural phase at larger Sm content.

It is worth to note that Fig. 2 shows the average *particle size* determined by SEM while Fig. 4 the average *crystallite size* determined by XRD using the Debye-Scherrer equation. In the case of XRD results (Fig. 4) all the calcined samples have systematically larger crystallite sizes compared with the not calcined, hence calcination favors crystallinity. In the case of the SEM results (Fig. 2) the data have an important degree of alternation between the calcined and not-calcined sizes, thus no conclusive affirmations

Table 1
Values of crystallite size and lattice parameter for both $Fe_{2-x}CoSm_xO_4$ particles before and after calcination.

Sm^{3+} content	Obtained particles		Calcined at 800 °C	
	Cristallite size (nm)	Lattice paremeter (±0.003 Å)	Cristallite size (nm)	Lattice paremeter (±0.003 Å)
0	16.0	8.416	23.5	8.400
0.05	14.9	8.414	19.2	8.401
0.1	19.7	8.422	22.3	8.412
0.15	24.3	8.414	25.5	8.392
0.2	23.4	8.417	24.2	8.389
0.3	20.3	8.366	22.4	8.362
0.4	21.6	8.413	24.0	8.374
0.5	20.5	8.410	27.0	8.373

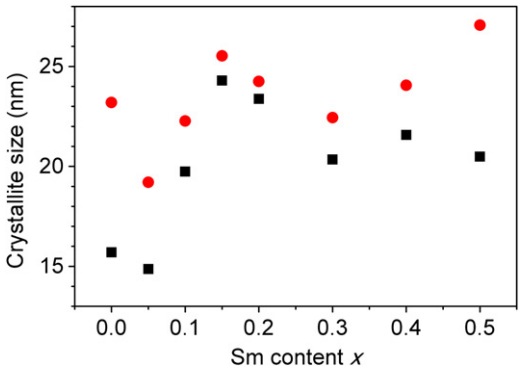

Fig. 4. Average crystalline size determined by Debye-Scherrer formula; for particles before (■) and after calcination (●).

can be extracted about comparing calcined versus not-calcined. Nevertheless, it is important to note that the particle size, obtained from statistical analysis of counting about 200–300 particles per SEM images, is always larger than the crystallite size for all samples (calcined or uncalcined) for all the designed compositions. It is a demonstration that the particles are composed of aggregates of crystallites since the average crystallite size is equal to the particle size only in case of monocrystalline particles.[19,20]

In spinel structures is known that the 220 peak intensity depends only on the A sites (tetrahedral) occupancy and the 222 peak intensity depends only on B sites (octahedral) occupancy[21]. For all the designed compositions and for both calcined and not calcined particles, the relative intensity of 220 and 222 peaks (normalized respect to 311) did not show a significant difference, and it cannot ensure that there is a variation on the inversion degree of the spinel structure when replacing Fe(III) by Sm(III). Despite of this, the ionic radius of Sm(III) (100 pm) is larger than the one of Fe(III) (64 pm) so the rare earth ions would replace Fe(III) occupying B sites and not A sites[16,17] producing great distortions on the crystalline structure and as a consequence of this, there is an increment on the lattice parameter. This effect is observed with small amounts of Sm (x=0.05–0.1) and also is reported in many works[16,17]. However, when the rare earth content x is higher than 0.1 for the non-calcined particles, the lattice constant oscillates, with a slightly decrease for large amounts of Sm(III) (x=0.4–0.5). Even though, for the calcined particles the lattice parameter decreases when Sm content increases further than 0.1. This effect can be attributed to the binding energy between Sm(III) and O^{2-} ions which is higher than the binding energy between Fe(III) and O^{2-} ions, thus with large amounts of Sm(III) and at high temperatures (800 °C) the perovskite phase $FeSmO_3$ starts to segregate. This second

phase compresses the spinel structure making the lattice parameter, the average crystal size and particle size (see 3.1) to decrease as the Sm(III) content becomes larger[11,16–18].

3.3. Magnetic measurements

All the synthesized particles have a ferromagnetic behavior. The magnetic hysteresis loops were measured for all the particles with applied fields between −10,000 and 10,000 Oe. Fig. 5(a) and (b) shows the first quadrant of the hysteresis loops for particles before and after the calcination respectively. Only curves for $x=0$, $x=0.1$, $x=0{,}2$ and $x=0.5$ are shown, for the sake of clarity. At first sight, it is clear that heat treatment enhance the magnetic behavior, comparing curves of the same Sm content before and after calcination (for a direct comparison, see supplementary material). To study in detail the magnetic behavior as a function of Sm content and heat treatment, the values of magnetization of saturation (M_s), remanent magnetization (M_r) and coercive field (H_c) were extracted from the hysteresis loops in all cases, and are shown in Table 2. M_s, M_r and H_c values for both series of particles are represented as a function of Sm(III) content x on Fig. 5a-c. For all the synthesized particles both values of M_s and M_r increases after the heat treatment, comparing batches with the same Sm content.

The behavior of M_s and M_r is similar: First, the values increase until reaching a maximum when the composition is near to $Fe_{1.9}CoSm_{0.1}O_4$. Then M_s and M_r decrease almost monotonically (except for the point at $x=0.3$). This behavior of the magnetic properties may have two important contributions. The first one is the replacement of Fe(III) ions by Sm(III) ions which have a smaller magnetic moment: 5.9 μ_B for Fe(III) vs. 1.7 μ_B for Sm(III)[11]. In $CoFe_2O_4$, Fe(III) ions occupy half A sites (tetrahedral) and half B sites (octahedral) while Co(II) ions occupy B sites. The magnetic moments of ions occupying A sites align anti parallel respect to ions occupying

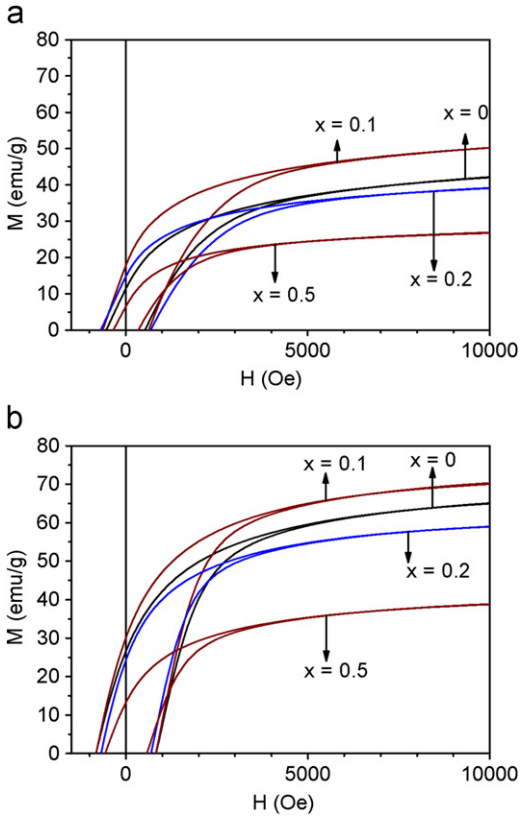

Fig. 5. Magnetization loops for $Fe_{2-x}CoSm_xO_4$ particles (a) before and (b) after calcination, for different Sm content.

Table 2
Ms, *Mr* and *Hc* values obtained from magnetization hysteresis loops for all compositions, before and after calcination.

Sm content x	Obtained particles			Calcined at 800 °C		
	M_s (emu/g)	M_r (emu/g)	H_c (Oe)	M_s (emu/g)	M_r (emu/g)	H_c (Oe)
0	42.1	11.4	536	64.9	26.7	823
0.05	51.6	11.8	333	65.2	26.1	702
0.1	50.2	17.7	655	70.0	30.2	797
0.15	36.4	14.3	932	57.5	23.6	655
0.2	39.1	14.7	687	50.5	24.3	683
0.3	28.7	8.3	422	32.1	10.7	574
0.4	30.9	8.5	400	39.9	14.1	540
0.5	26.9	6.5	343	38.9	13.3	568

B sites.[22] When samarium is added, the Sm(III) ions replace Fe(III) ions in B sites since the ionic radius of Sm(III) is too large to occupy tetrahedral sites (as indicated in Section 3.3). Considering that the magnetic moment of Sm(III) is about 0.29 times that of Fe(III), the main conclusion is that the magnetic moment per unit cell is expected to decrease after replacing Fe(III) by Sm(III). However, it is not straightforward to extrapolate the variation of M_s and M_r from the above considerations, as other factors have strong influence also (such as crystallite and particle sizes).[23] Furthermore, Sm(III) ions posses a higher molecular mass than Fe(III) ions (150.36 and 55.85 g/mol respectively). That would yield a monotonically decrease in the magnetization per unit of mass over the entire x range.

Another contribution is the presence of an amorphous phase on the surface of the particles, acting as a shell with non-magnetic moment[24]. When the particle size decreases the surface-volume ratio increases, lowering the magnetization per unit of volume or mass. As the mean particle size increase up to $x=0.15$ and then decrease from 0.15 to 0.5, one would expect the saturation and remanence have a similar behavior. A third element affecting the magnetic properties is the presence of a perovskite phase for x between 0.2 and 0.5 for the calcined particles. This phase is known to be non-magnetic[11,16] so the apparent mass magnetic saturation is also reduced in this range. The observed behavior is a consequence of these three effects combined, in which there is a first slightly increase in M_s and M_r and then a marked decrease in their values. The enhanced values of M_s and M_r for the calcined particles are directly related to their higher degree of crystallinity, reducing the amorphous surface shell on them. In this way, heat treatment plays an important role in the stabilization and enhancement of magnetic saturation and remanence.

Concerning the coercive field behavior (H_c), it is expected to reduce when the mean particle size decrease, since the particles are in the monodomain regime[25,26]. Then, taking into account the behavior of the particle size with x, the coercive field is expected to grow slightly up to $x=0.1$ and then decrease monotonically. This behavior is observed, but with a high dispersion of points, in the non-calcined particles. For the calcined particles, only a slight (less dispersed) drop in coercive field is observed. It is worth to note that the assumption that the particles are in the monodomain regime is based on measurements for the parent compound. Up to our knowledge, experiments for particles with Sm substitution were not performed, and that will be elucidated in further works. Fig. 6

3.4. Morphology of PDMS-NPs composites

Cylindrical PDMS-$Fe_{2-x}CoSm_xO_4$ elastic composites were obtained after curing the base polymer, cross linker and nanoparticle mixture in the presence of a uniform magnetic field. The magnetic material gets aligned as a consequence of the dipolar interaction between particles; forming macroscopic needles (micrometric columnar

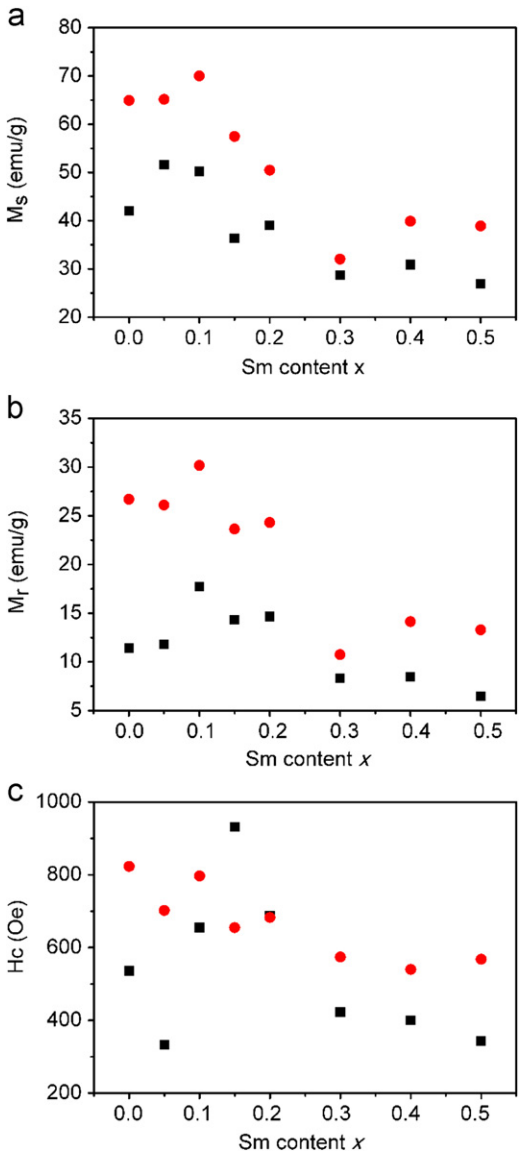

Fig. 6. Effect of Sm content x in magnetic properties of $Fe_{2-x}CoSm_xO_4$ particles: variation of M_s(a) M_r(b) and H_C (c) extracted from magnetization loops of $Fe_{2-x}CoSm_xO_4$ particles before (■) and after calcination (●).

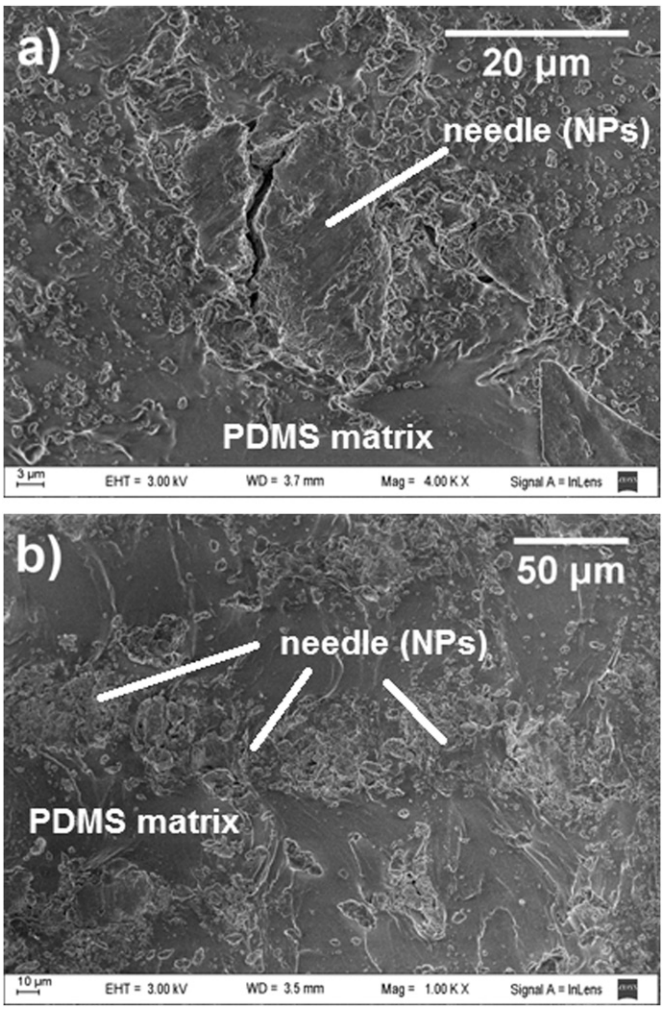

Fig. 7. SEM image of the obtained composites showing the formed needles of micrometric size. (a) Top view of a needle surrounded of a PDMS matrix. (b) Lateral view of a needle surrounded of PDMS matrix and other needles.

structures) oriented parallel to the magnetic field applied during curing, as observed in recent papers[14,15] (see Fig. 7). The elastic and magnetic properties of these structured composites are characterized and discussed in the next sections. SEM images showing the formed needles are presented in Fig. 7. Fig. 7a shows a top view of one of the columnar structures formed. As it is seen, the cross-section is irregular, with a mean diameter of approximately 20 μm. Fig. 7b shows a lateral cut of a region in which three needles are observed.

3.5. Magnetic anisotropy and time relaxation of composites

In order to investigate the magnetic anisotropy of the composites, magnetic remanence and time relaxation experiments were performed for PDMS-$Fe_{1.9}CoSm_{0.1}O_4$ structured composites, prepared with calcined and not calcined NPs, as a function of the angle of the applied field with respect to the needle direction (that is, the direction of the curing field). The experiment consists in applying a high magnetic field (10,000 Oe) at a given angle, so that the sample reaches its magnetic saturation. Then, the magnetic field is removed and the magnetic moment of the sample was registered as a function of elapsed time (t). The first point registered by the magnetometer (approximately 6 s after the field is removed) is taken as the M_r for every angle. The complete M vs. t curve is the magnetic relaxation for these conditions. It is known that the time dependence of the magnetization is given by[27]

$$M(t,T)/M_0 = 1 - S(t,T)\ln(t/\tau_0) \quad (1)$$

where M_0 is the magnetization for $t=\tau_0$, and $S(t,T)$ is the magnetic viscosity that depends on time (negligible) and temperature (T). By plotting M/M_0 as a function of $\ln(t)$ a linear dependence with slope $-S$ is expected, as it is shown on Fig. 8 for the PDMS-$Fe_{1.9}CoSm_{0.1}O_4$ composite.

On Fig. 9a we show the angular dependence of M_r (normalized to Ms for each α, measured from the needle direction) for both PDMS-$Fe_{1.9}CoSm_{0.1}O_4$ composites elaborated with calcined and not-calcined NPs. For both composites a *cosine* dependence respect to α is observed, with a maximum of M_r/M_s when $\alpha=0^\circ$ (field parallel to the formed needles) and a minimum when $\alpha=90^\circ$ (field perpendicular to the needles). Also for both composites a difference of 25% is observed on the normalized M_r when $\alpha=0^\circ$ respect to its value when $\alpha=90^\circ$. Moreover, for the composite elaborated with the calcined NPs the normalized M_r is 65% higher than the respective values of M_r for the composite with the not calcined particles for all α.

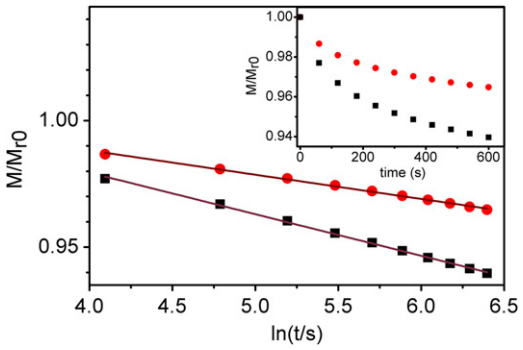

Fig. 8. Time relaxation experiment for PDMS-$Fe_{1.9}CoSm_{0.1}O_4$ NPs (10% *w*/*w*) composites. (■) using uncalcined particles. (●) using calcined particles. In both cases, prior to the measurement, a magnetic field is applied parallel to the needles, and then removed. M_r decays linear with ln(t). The inset of the figure shows the measured values. The main panel is the semilog graph with the tendency lines of Eq. (1) indicated.

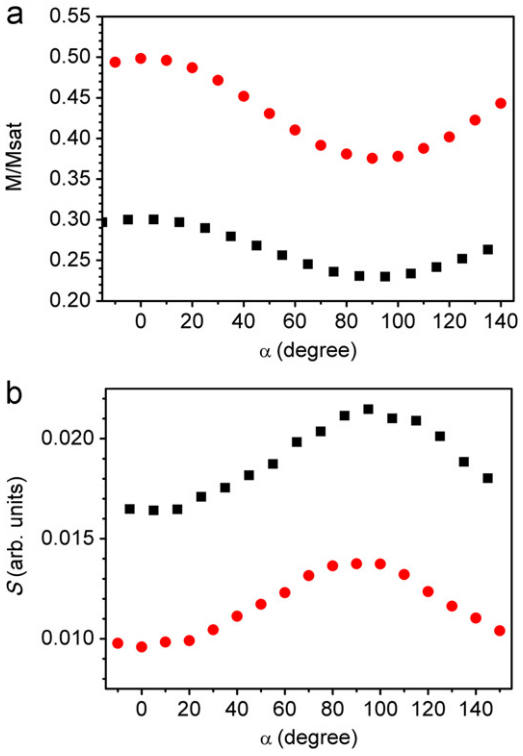

Fig. 9. (a) Remanent magnetization (normalized to $M_{s,\alpha}$) vs angle of the applied field with respect to the needle direction (α), for PDMS-$Fe_{1.9}CoSm_{0.1}O_4$ composites (10% *w*/*w*) using particles with and without heat treatment. (b) Magnetic viscosity as a function of α for PDMS-$Fe_{1.9}CoSm_{0.1}O_4$ composites. (●) Composite prepared with calcined particles. (■) Composite prepared with uncalcined particles.

On Fig. 9(b) the obtained values of S are plotted, as a function of α for both composites, and a *sine* dependence is observed in both cases, with a maximum value for S when $\alpha=90^\circ$ and a minimum when $\alpha=0^\circ$. Even though, the values of S for the composite elaborated with the calcined NPs are at least 35% smaller than those obtained for the composite with the not calcined NPs for all α. Fig. 9(a) and (b) both point in the same direction. Firstly, there exist a marked magnetic anisotropy on the structured composites, that could be due to either the increased magnetic dipolar interaction of particles arranged in a columnar structure when the field is applied parallel to it, or the individual easy axis distribution of the particles that was frozen with a preferred orientation during curing the polymer. This causes that the time relaxation of the composite with the calcined nanoparticles is slower than the one of the composite with the uncalcined particles, and for both composites the relaxation is faster when the applied field is perpendicular to the needles. Furthermore, composites structured with calcined particles have slower dynamics and higher magnetic remanence. It could be due to the enhanced crystallinity of individual particles that favors magnetic interaction between them, by reducing the thickness of the particles' amorphous layer.

3.6. Elastic measurements

Compression experiments on the composites were performed with the aim to determine the influence of the formed needles in the elastic properties of the PDMS-NPs composites. The Young modulus was determined for different composites elaborated with NPs with different content of Sm. A cyclic compression experiment is shown in Fig. 10a in which it can be seen that composite does not deform after three cycles of slow compression and fast decompression (instantaneously at the experiment time scale) and the same magnitude of strength is required to achieve three consecutive cycles of compression. On Fig. 10b is shown a test of elastic time relaxation in which the sample is compressed up to 20% strain and then the sample is kept at that strain for 60 s. In both Fig. 10(a and b) it can be seen that more pressure is required to compress the composite in the direction parallel to the formed needles rather than in the perpendicular direction, in concordance with our earlier studies[14,15]. Analyzing the dependence of the thickness variation with respect to the applied pressure, the Young modulus (E) can be obtained from an exponential fit [14,15]. In Fig. 10c the strain-stress curves are presented for PDMS-$Fe_{1.8}CoSm_{0.2}O_4$ NPs (10% *w*/*w*) in both directions parallel and perpendicular to the formed needles, where there is noticed that E measured parallel to the needles ($E_{//}$) is almost twice in magnitude larger than the one measured perpendicular to the needles ($E_\perp$).

The recovered values of $E_{//}$ and $E_\perp$ can be compared with E_m, the Young's modulus of the cured polymer matrix in absence of filler ($E_m=7$ cm^2/KgF [14,15]) for 10% *w*/*w* composites. While $E_\perp$ remains similar to E_m, a significant increase of $E_{//}$ is observed, with values between 11 and 15 cm^2/KgF (non-calcined particles were used) with no trends observed as function of Sm content. Thus, the structured composites display a significant elastic anisotropy, even for relative low filler loading, with percentage anisotropy change ($100(E_{//}-E_\perp)/E_\perp$) about 50%.

4. Conclusions

As it can be seen on SEM images the as-prepared particles posses irregular spherical shape. These particles have inverse spinel crystalline structure in their core and seem to have an amorphous structure on the surface. After calcination at 800 °C the degree of crystallinity of the particles increases. This behavior can be seen in SEM images, where the borders of the particles become well defined, and also in XRD diffractograms in which the noise decreases and the peaks become narrower. For both sets of particles, calcined and not calcined, the average size distribution could be fitted to lognormal curves.

For all the designed compositions, the as-prepared particles do not show phase segregation, even for large amount of Sm(III). When the particles are exposed to high temperatures, thermal energy is used to form Sm(III)-O^{2-} bonds. As a result a stable perovskite phase of $FeSmO_3$ starts to segregate when Sm(III) content x is 0.2 or higher. This foreign perovskite phase makes the spinel lattice to contract, explaining the observed tendency

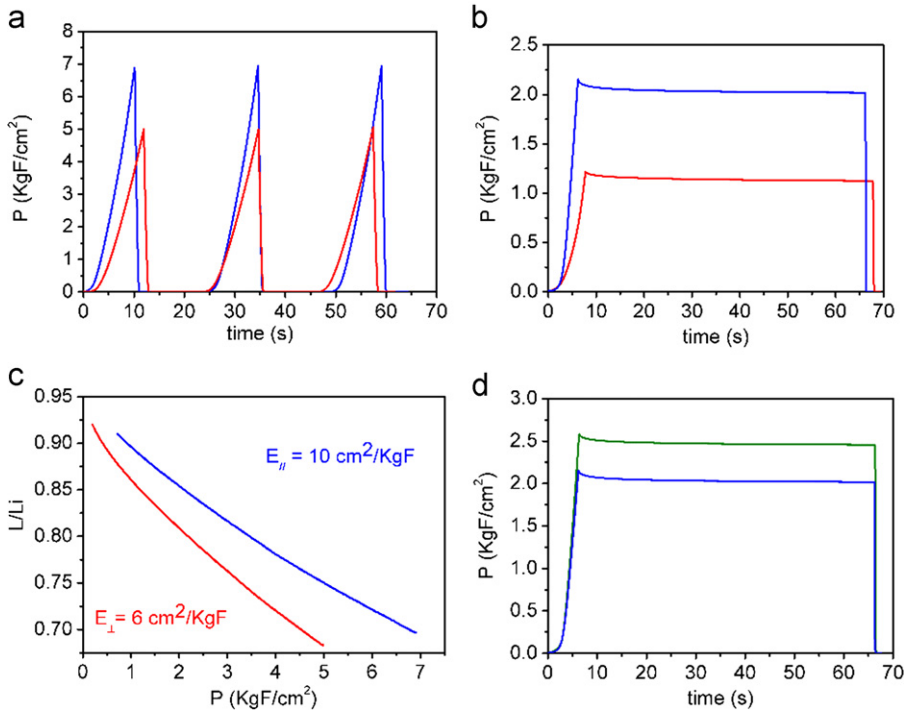

Fig. 10. Texture analysis of PDMS-NPs composites. (a) slow compression, fast decompression (strain 30%) on PDMS-NPs (10% *w/w*, $x=0.2$, non-calcined) composite (b) time relaxation experiment (strain 20%, relaxation time 60 s) on PDMS-NPs (10% *w/w*, $x=0.3$, non-calcined) composite. (c) Relative thickness (L/Li) vs. applied pressure (P) for PDMS-NPs (10% *w/w*, $x=0.2$, non-calcined) composite. (---) pressure applied parallel to the needles. (---) Pressure applied perpendicular to the needles. (d) Time relaxation experiment (strain 20%, relaxation time 60 s) for PDMS-NPs (10% *w/w*, $x=0.1$) (---) composite prepared with uncalcined NPs. (---) composite prepared with calcined particles; in both cases the applied pressure is parallel to the needles.

for the lattice parameter of the calcined particles. Following this, after the heat treatment the degree of crystallinity of the particles is increased.

The behavior of the magnetic parameters of the particles have several contributions: the average particle size, the Sm(III) content and the presence of the perovskite (non-magnetic) phase. According to this, a combined effect is proposed to explain the tendency shown on Fig. 5a–b: when Sm(III) is low ($x=0$–0.15) and as the Sm (III) amount increases, the particle size increases and the effect of amorphous non-magnetic shell losses weight. This is observed for both calcined and not calcined particles. When Sm(III) content is mid and high ($x=0.2$–0.5) other effects contribute to the decrease of M_s and M_r: the replacement of Fe(III) by Sm (III) (observed in both sets of particles), and the segregation of a non magnetic perovskite phase (observed only in calcined particles). Even though, analyzing the dependence of M_s and M_r as a function of the particle size, these values reach a maximum when the Sm(III) content x is near to $0.1-0.15$.

Summarizing all the mentioned above, it can be concluded that Sm(III) ions have a limited solubility on the Fe_2CoO_4 spinel lattice due to the large ionic radius of the dopant. As mentioned before, Sm(III) replace Fe(III) in the B sites, making great distortions on the spinel lattice. When the particles are exposed to high temperatures, the excess of Sm(III) ions segregate as $FeSmO_3$.

The role of heat treatment is shown to be very useful to enhance magnetic saturation and remanence, to stabilize structural properties and to increase crystallinity of particles. In the composites, time relaxation experiments show that the magnetic moment decreases faster when the applied field is perpendicular to the needles. When calcined particles are used for preparing the composites, the time relaxation is slower, and as a result of this, the magnetic viscosity is lower in magnitude for these samples. The elastic measurements show that the formed needles after curing the samples under an external magnetic field (that induces spatial structuration of the composites) yields an anisotropic elasticity: the Young modulus is always larger when is measured parallel to the needles. The magnetic anisotropy is also a consequence of the magnetic structuration of the composites, and can be attributed to the enhanced magnetic dipolar interaction within an individual needle or the freezing of an anisotrtopic magnetic easy-axis distribution of the particles.

Acknowledgments

PSA, GJ and RMN are research members of the National Council of Research and Technology (CONICET, Argentina). MMR is a doctoral fellowship of CONICET. JLM received a fellowship of the University of Buenos Aires (UBA). Financial support was received from the National Agency for Promotion of Science and Technology (ANPCYT, PICT 2011-0377).

Appendix A. Supporting information

Supplementary data associated with this article can be found in the online version at http://dx.doi.org/10.1016/j.jmmm.2012.09.020.

References

[1] M. Johannsen, U. Gneveckow, B. Thiesen, K. Taymoorian, C.H. Cho, N. Waldöfner, R. Scholz, A. Jordan, S.A. Loening, P. Wust, European Urology 52 (2007) 1653.
[2] K.E. Scarberry, E.B. Dickerson, Z.J. Zhang, B.B. Benigno, J.F. McDonald, Nanomedicine: Nanotechnology, Biology and Medicine 6 (2010) 399.
[3] C. Sun, J.S.H. Lee, M. Zhang, Advanced Drug Delivery Reviews 60 (2008) 1252.
[4] H.J. Chen, Y.M. Wang, J.M. Qu, R.Y. Hong, H.Z. Li, Applied Surface Science 257 (2011) 10802.

[5] I.G. Yáñez-Flores, R. Betancourt-Galindo, J.A.M. Aquino, O. Rodríguez-Fernández, Journal of Non-Crystalline Solids 353 (2007) 799.
[6] X. Dong, M. Yu, C. Liao, W. Chen, Transactions of Nonferrous Metals Society of China 19 (Supplement 3) (2009) s611.
[7] K.L. Phan, A. Mauritz, F.G.A. Homburg, Sensors and Actuators A: Physical 145–146 (2008) 109.
[8] M. Farshad, A. Benine, Polymer Testing 23 (2004) 347.
[9] K.W. Oh, C.H. Ahn, Comprehensive Microsystems, Elsevier, Oxford, 2008 pp. 39–68.
[10] Z. Varga, G. Filipcsei, M. Zrínyi, Polymer 46 (2005) 7779.
[11] M.M. Rashad, R.M. Mohamed, H. El-Shall, Journal of Materials Processing Technology 198 (2008) 139.
[12] A. Cabañas, J.A. Darr, E. Lester, M. Poliakoff, Journal of Materials Chemistry 11 (2001) 561.
[13] V. da, R. Caffarena, T. Ogasawara, Materials Research 6 (2003) 569.
[14] P. Soledad Antonel, G. Jorge, O.E. Perez, A. Butera, A. Gabriela Leyva, R.Martín Negri, Journal of Applied Physics 110 (2011).
[15] J.L. Mietta, M.M. Ruiz, P.S. Antonel, O.E. Perez, A. Butera, G. Jorge, R.M. Negri, Langmuir 28 (2012) 6985.
[16] L. Guo, X. Shen, F. Song, L. Lin, Y. Zhu, Materials Chemistry and Physics 129 (2011) 943.
[17] N. Rezlescu, E. Rezlescu, Solid State Communications 88 (1993) 139.
[18] Z. Peng, X. Fu, H. Ge, Z. Fu, C. Wang, L. Qi, H. Miao, Journal of Magnetism and Magnetic Materials 323 (2011) 2513.
[19] A.W. Burton, K. Ong, T. Rea, I.Y. Chan, Microporous and Mesoporous Materials 117 (2009) 75.
[20] S.J.S. Qazi, A.R. Rennie, J.K. Cockcroft, M. Vickers, Journal of Colloid and Interface Science 338 (2009) 105.
[21] B.P. Ladgaonkar, A.S. Vaingankar, Materials Chemistry and Physics 56 (1998) 280.
[22] R. Masrour, M. Hamedoun, A. Benyoussef, Journal of Alloys and Compounds 503 (2010) 299.
[23] J. Li, H. Yuan, G. Li, Y. Liu, J. Leng, Journal of Magnetism and Magnetic Materials 332 (2010) 3396;
S.E. Jacobo, S. Duhalde, H.R. Bertorello, Journal of Magnetism and Magnetic Materials 272 (2004) 2253.
[24] R.H. Kodama, Journal of Magnetism and Magnetic Materials 200 (1999) 359.
[25] K. Maaz, A. Mumtaz, S.K. Hasanain, A. Ceylan, Journal of Magnetism and Magnetic Materials 308 (2007) 289.
[26] C.N. Chinnasamy, B. Jeyadevan, K. Shinoda, K. Tohji, D.J. Djayaprawira, M. Takahashi, R. Justin Joseyphus, A. Narayanasamy, Applied Physics Letters 83 (2003) 2862.
[27] M. Knobel, W.C. Nunes, L.M. Socolovsky, E. De Biasi, J.M. Vargas, J.C. Denardin, Journal of Nanoscience and Nanotechnology 8 (2008) 2836.